



A multipurpose, adolescent idiopathic scoliosis-specific, short MRI protocol: A feasibility study in volunteers

Yulia M. Shcherbakova^{a,*}, Peter P.G. Lafranca^b, Wouter Foppen^c, Tijl A. van der Velden^{a,d}, Rutger A.J. Nivelstein^c, Rene M. Castelein^b, Keita Ito^{b,e}, Peter R. Seevinck^{a,d}, Tom P. C. Schlosser^b

^a Department of Radiology, Image Sciences Institute, UMC Utrecht, Utrecht, Netherlands

^b Department of Orthopaedic Surgery, UMC Utrecht, Utrecht, Netherlands

^c Department of Radiology & Nuclear Medicine, Division Imaging & Oncology, UMC Utrecht, Utrecht, Netherlands

^d MRiguidance B.V., Utrecht, Netherlands

^e Department of Biomedical Engineering, Eindhoven University of Technology, Eindhoven, Netherlands

ARTICLE INFO

Keywords:

Adolescent Idiopathic Scoliosis
Scoliosis-specific
Multipurpose MRI-protocol
Short MRI-protocol
Radiation-free
Spinal navigation

ABSTRACT

Introduction: Visualization of scoliosis typically requires ionizing radiation (radiography and CT) to visualize bony anatomy. MRI is often additionally performed to screen for neural axis abnormalities. We propose a 14-minutes radiation-free scoliosis-specific MRI protocol, which combines MRI and MRI-based synthetic CT images to visualize soft and osseous structures in one examination. We assess the ability of the protocol to visualize landmarks needed to detect 3D patho-anatomical changes, screen for neural axis abnormalities, and perform surgical planning and navigation.

Methods: 18 adult volunteers were scanned on 1.5 T MR-scanner using 3D T2-weighted and synthetic CT sequences. A predefined checklist of relevant landmarks was used for the parameter assessment by three readers. Parameters included Cobb angles, rotation, torsion, segmental height, area and centroids of Nucleus Pulposus and Intervertebral Disc. Precision, reliability and agreement between the readers measurements were evaluated. **Results:** 91 % of Likert-based questions scored ≥ 4 , indicating moderate to high confidence. Precision of 3D dot positioning was 1.0 mm. Precision of angle measurement was 0.6° (ICC 0.98). Precision of vertebral and IVD height measurements was 0.4 mm (ICC 0.99). Precision of area measurement for NP was 8 mm^2 (ICC 0.55) and for IVD 18 mm^2 (ICC 0.62) for IVD. Precision of centroid measurement for NP was 1.3 mm (ICC 0.88–0.92) and for IVD 1.1 mm (ICC 0.88–0.91).

Conclusions: The proposed MRI protocol with synthetic CT reconstructions, has high precision, reliability and agreement between the readers for multiple scoliosis-specific measurements. It can be used to study scoliosis etiopathogenesis and to assess 3D spinal morphology.

1. Introduction

Adolescent idiopathic scoliosis (AIS) is a 3D spinal deformity affecting 2–4 % of the population [1–3]. AIS is the most common type of pediatric scoliosis, affecting previously healthy children during the adolescent growth spurt. Non-idiopathic scoliosis, such as neuromuscular or syndromic scoliosis develops in children with neuromuscular

diseases or specific syndromes. During growth, the spinal deformity can severely progress, which can significantly reduce the patient's quality of life. Visualization of AIS is typically done with standing full spine posterior-anterior and lateral radiographs to assess the curve's magnitude and eventual progression for AIS evaluation and surgical planning. Magnetic Resonance Imaging (MRI) can be performed additionally to analyze potential abnormalities of the spinal cord or the brain stem such

Abbreviations: AI, Artificial Intelligence; AIS, Adolescent Idiopathic Scoliosis; CT, Computed Tomography; FOV, Field Of View; ICC, Intra-class Correlation Coefficient; IVD, Intervertebral Disc; NP, Nucleus Pulposus; MRI, Magnetic Resonance Imaging; ROI, Region of interest; sCT, Synthetic Computed Tomography; TSE, Turbo Spin Echo; 3D, Three-dimensional.

* Corresponding author.

E-mail address: Y.M.Shcherbakova@umcutrecht.nl (Y.M. Shcherbakova).

<https://doi.org/10.1016/j.ejrad.2024.111542>

Received 20 March 2024; Accepted 31 May 2024

Available online 1 June 2024

0720-048X/© 2024 The Authors. Published by Elsevier B.V. This is an open access article under the CC BY license (<http://creativecommons.org/licenses/by/4.0/>).

as Chiari-malformation, syringomyelia or tethered cord [4–6]. This is commonly done with a whole spinal cord MRI protocol, consisting of multiple sequences, repeated usually in two stations, depending on how tall the patient is, with a total scan duration varying from 40 to 90 min [7]. In younger children this often requires general anesthesia. Additional computed tomography (CT) scans are sometimes performed in children with complex osseous deformations, and pre-operative CT scans are nowadays increasingly used for surgical planning and spinal navigation surgery.

The multiple radiographs performed over years in AIS patients combined with an increased use of CT scans for planning and navigation lead to a significant radiation exposure in these young children [8–10], with an associated risk of radiation-related cancer of one for every 1000 scoliosis patients treated [11]. Although the radiation burden with modern and sophisticated equipment is lower, it is still important to minimize the radiation exposure, particularly in children, who have a higher risk of developing cancer due to ionizing radiation [11–16]. Furthermore, in research studies on normal spinal development in healthy children, or on early changes in children that later develop scoliosis, the use of ionizing radiation is more than a minimal burden and therefore ethically not acceptable [17].

MRI traditionally does not allow for an accurate 3D visualization of cortical bones like CT does, but the development of synthetic CT (sCT) from MRI images using artificial intelligence (AI) can be an alternative to conventional CT [18]. Generated sCT images have been proven to be equivalent to conventional CT for the evaluation of osseous morphology in the hip [19], cervical spine [20], sacroiliac joint for adults as well as children [21–23], and for surgical planning and navigation in the lumbar spine [24–26]. Given the absence of ionizing radiation and the fact that all relevant information on osseous and soft tissue structures can be obtained in only one imaging modality, this approach is especially relevant for the complex spinal anatomy where the surgeon requires information about the 3D bony anatomy, the spinal cord, nerve roots, and major vessels at the same time. Certainly, sCT generation is beneficial for the pediatric population [27–29], and for patients requiring regular follow-up scans.

In this work, we aim for a radiation-free short imaging protocol that minimizes the burden to pediatric patients and allows to visualize all landmarks to detect patho-anatomical changes in the bone and soft-tissues in children at risk for scoliosis, to screen for neural axis abnormalities, and to perform surgical planning and navigation in patients with more severe scoliosis. For that, we present a 14-min scoliosis-specific, multipurpose MRI protocol. The protocol consists of 3D T2-weighted Turbo Spin Echo (TSE) scans of the cervical, thoracic and lumbar spine, and an MRI-based sCT scan of T3–L4. The protocol was developed specifically for AIS patients with the goal to fulfill multiple specific purposes in a short scanning time. The purpose of this study was to assess the feasibility of the proposed multi-purpose MRI protocol and to demonstrate its sufficiency to fulfill multiple purposes, by systematic quantitative and qualitative assessment of pilot MRI images of young adult volunteers.

2. Methods

18 healthy adult volunteers (average age 26, range 21–37 years old) participated in this study and written informed consent was signed by all participants. The study was approved by the local institutional review board. The volunteers were scanned using a clinical 1.5 T MRI scanner (Philips Healthcare, Best, NL) using the base head coil and the built-in posterior coil. MRI images were acquired using the protocol described in Table 1. Synthetic CT images were generated using BoneMRI V1.5 (MRGuidance BV, Utrecht, The Netherlands). Cervical T2-weighted images were obtained in 5 volunteers using the base head coil and the built-in posterior coil.

A checklist of all relevant landmarks for detection of early stages of scoliosis, screening for neural axis abnormalities, surgical planning,

Table 1

The protocol parameter settings for the sequences included in the protocol and the amount of the volunteers scanned.

Sequence	3D Sag T2w TSET-spine	3D Sag RF- spoiledmulti-echo- gradient-echo “BoneMRI”T-spine	3D Sag T2w TSEC-spine
Field Of View (FOV)	220 × 420 × 100 mm ³ (AP × FH × RL)	220 × 420 × 100 mm ³ (AP × FH × RL)	280 × 280 × 60 mm ³ (AP × FH × RL)
Acquisition Voxel size	1 × 1 × 1 mm ³ 0.625 × 0.625	1 × 1 × 2 mm ³ 0.625 × 0.625 × 1	0.9 × 1 × 1.2 mm ³
Reconstruction voxel size	× 1 mm ³	mm ³	0.435 × 0.435 × 0.6 mm ³
Flip Angle (FA)	90°	10°	90°
Repetition Time (TR)	1200 ms	7 ms	1300 ms
Echo Time (TE)	109 ms	2.1 ms/4.2 ms	113 ms
Phase	Feet-Head	Feet-Head	Feet-Head
Encodingdirection			
Numbers of Signal	1	2	1
Averages (NSA)			
Acceleration	SENSE 2.2 in FHSense 2.2 in RL	SENSE 1.2 in FH	SENSE 2.2 in FHSense 2.2 in RL
Acquisitiontime	06:14 min	04:48 min	02:27 min
Number of volunteers	18	18	5

spinal navigation surgery was predefined based on available literature and the input of two experienced scoliosis surgeons and researchers on scoliosis etiopathogenesis (see Fig. 1). Based on the checklist, a detailed reader manual was prepared for structured data assessment and provided in the [supplementary materials](#).

The assessment of the volunteer MRI data was performed digitally, using the reader manual, by three independent readers: a musculo-skeletal radiologist, a spine surgeon, and an orthopaedic resident. Checklists were filled in using in-house developed software for online testing with 3D radiological images (Vquest, <https://vquest.nl>) [30]. Readers were asked to answer five types of questions:

- (1) Likert-based multiple-choice questions to assess image quality for detecting certain landmarks – relevant parameters 3, 9, 11–18 in Fig. 1.
- (2) Placing a line based on landmarks for angular measurements (Cobb angle, Apical axial rotation, and local vertebral body torsion) – relevant parameters 1, 2, 4, 7 in Fig. 1.
- (3) Placing multiple dots (markers) at the position of 2D landmarks for vertebral and intervertebral disc (IVD) height measurements – relevant parameters 5, 6 in Fig. 1.
- (4) Placing a hand-drawn contour based on landmarks – relevant parameters 8 in Fig. 1.
- (5) Placing multiple dots (markers) at the position of 3D landmarks – relevant parameters 10 in Fig. 1.

For the Likert-based multiple-choice type 1 questions, the readers were asked to rate the quality of the MRI images with regard to their confidence in the ability to determine, detect, or classify the landmarks using those images. A 5-point Likert scale was used for the assessment of images. For each question, the mean score among the readers was calculated, as well as the percentage with scores ≥ 4 and score = 5.

For questions of type 2–5, quantitative analysis of the reader's answers was performed. First, to assess, how close the readers' answers (in the form of 3D point coordinates, or calculated parameters such as angles, vertebral and IVD heights, ROI areas and ROI centroids) are to each other, the precision was evaluated as described below for each individual type of questions. Next, to assess the reproducibility of the clinically relevant parameters, calculated using the readers' answers, such as the angle, vertebral and IVD heights, ROI area and ROI centroid, both the reliability and the agreement between the readers' measurements




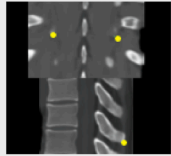


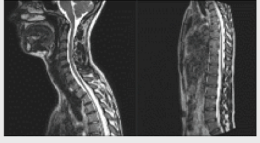


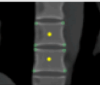

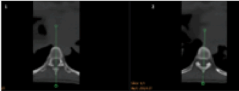
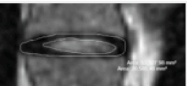
Relevant Parameter	Answer and the result	Method	Example	Relevant Parameter	Answer and the result	Method	Example
Detection of early patho-anatomical changes: Regional measures							
1. Coronal Cobb angle	2 lines drawn 2 angles with the reference horizontal line calculated	In two provided 2D images, draw a line parallel to the upper endplate of the marked vertebra, and a line parallel to the lower endplate of the marked vertebra.		9. Pfirrmann grade for IVD degeneration	Likert scale answer: 1-5 How confident are you that you are able to classify the IVD degeneration according to the Pfirrmann grade in the provided 3D image, on a 5-point Likert scale?		
2. Sagittal Cobb angle	4 lines drawn 4 angles with the reference horizontal line calculated	In four provided 2D images, draw a line parallel to the upper endplate of the marked vertebra, and a line parallel to the lower endplate of the marked vertebra.		10. Ligaments attachments	3 dots are placed Coordinates of 3 dots are calculated	In the provided 3D images, on the middle vertebra, set 2 dots at the caudal side of the tips of transverse processes and one dot at the caudal side of the tip of spinous process. The dots should not be placed outside of the cortical bone.	
3. Apical vertebral level	Likert scale answer: 1-5	In the provided 3D image, if there was a scoliosis, how confident are you that you are able to identify the apical vertebral level, based on a 5-point Likert scale?		Screening for underlying neural axis abnormalities			
4. Apical axial rotation	A line placed An angle with the reference vertical line calculated	In the provided 2D image, draw a line through the center of the vertebra and the center of the spinal canal.		Presence/absence of the underlying neural axis abnormalities: 11. Chiari malformation 12. Syringomyelia 13. Tethered cord	Likert scale answer: 1-5 How confident are you that you are able to detect (if it was present) the underlying neural axis abnormality - Chiari malformation/ syringomyelia/ tethered cord, in the provided 3D images, on a 5-point Likert scale?		
Detection of early patho-anatomical changes: Local measures of vertebral bodies and posterior elements				Surgical planning/spinal navigation surgery			
5.1 Vertebral body A-P height ratio 5.2 IVD A-P height ratio	8 dots placed 12 parameters calculated: vertebral and IVD heights	In the provided 2D image, set 8 dots on the corners of the two marked vertebrae. The dots should not be placed outside of the cortical bone.		14. Screening for congenital osseous abnormalities	Likert scale answer: 1-5 How confident are you that you are able to detect (if they were present) any underlying congenital osseous abnormalities in the provided 3D image, on a 5-point Likert scale?		
6.1 Vertebral body L-R height ratio 6.2 IVD L-R height ratio	8 dots placed 12 parameters calculated: vertebral and IVD heights	In the provided 2D image, set 8 dots on the corners of the two marked vertebrae. The dots should not be placed outside of the cortical bone.		15. Pedicle screw planning – for thoracic spine 16. Spinal navigation – for thoracic spine 17. Pedicle screw planning – for lumbar spine 18. Spinal navigation – for lumbar spine	Likert scale answer: 1-5 How confident are you that: - you are able to determine the 3D orientation of the pedicle for thoracic/lumbar spine, - the surface of the posterior elements is well enough visualized for surgical navigation for thoracic/lumbar spine. on provided 3D image, on a 5-point Likert scale?		
7.1 Local geometric vertebral body torsion 7.2 Intervertebral axial rotation 7.3 Local geometric IVD torsion	4 lines drawn 4 angles with the reference vertical line calculated	In four provided 2D images, draw a line through the center of the vertebra and the center of the spinal canal.					
8.1 IVD volume 8.2 Nucleus pulposus position and volume 8.3 Annulus fibrosus volume	2 contours are drawn 4 parameters calculated	In three coronal 2D images draw: first, a contour of the NP and second, a contour of the outer border of the IVD.					

Fig. 1. The checklist of all relevant landmarks with the parameters, answer options, methods, and image examples.

were evaluated. The reliability was evaluated by calculation the intra-class correlation coefficient (ICC) [31], using type 'C-1' (consistency ICC in the presence of bias). The agreement was evaluated using Jones plots [32], where the difference in the measurements between three readers was plotted versus the average of the measurement. The mean difference and the 95 % limits of agreements were calculated as well, representing how different an individual reader could be compared with the mean measurement of all the readers.

2.1. Placing a line based on landmarks

For each line placed by the readers, the angle between the line and the reference line was calculated (further referred as the angle measured by the readers). For each specific question, the average angle was calculated over the readers. The precision in angle measurement was defined as the mean value of the absolute differences between each readers' measured angle and the average angle, and was calculated for each specific question using Eq. [1]. Then all the angles were combined (representing the Cobb angle, apical axial rotation, and local vertebral body torsion), and the overall precision, as well as the reliability and the agreement between the readers were evaluated.

$$Precision = \frac{\sum_{i=1}^3 abs(Angle_i - \overline{Angle})}{3}, \quad \text{where } \overline{Angle} = \frac{\sum_{i=1}^3 Angle_i}{3} \quad (1)$$

2.2. Placing multiple dots at the position of 2D landmarks

For measuring vertebral body and IVD dimensions, the readers were asked to place eight dots at the corners of two selected adjacent vertebrae (T8-T9) using mid-sagittal and mid-coronal images: vertebra # 1 (T8) anterior, posterior, right, left heights, vertebra # 2 (T9) anterior, posterior, right, left heights, IVD (T8-T9) anterior, posterior, right, left heights (further referred as the heights measured by the readers). For each specific question, the average IVD and vertebral heights were calculated over the readers. The precision in IVD and vertebral height measurement was defined as the mean value of the absolute differences between each readers' measured height and the average height (per parameter) and was calculated for each specific question using Eq. (2). The overall precision, as well as the reliability and the agreement between the readers were evaluated.

$$Precision = \frac{\sum_{i=1}^3 abs(Height_i - \overline{Height})}{3}, \quad \text{where } \overline{Height} = \frac{\sum_{i=1}^3 Height_i}{3} \quad (2)$$

2.3. Placing a hand-drawn contour based on landmarks

The readers were asked to draw two contours, or regions of interest (ROIs) on the NP (ROI 1) and the outer border of the IVD (ROI 2) on three adjacent coronal slices, using 3D Sag T2w TSE images. The ROIs placed on the middle slice were used to calculate two parameters – the

area and the centroid (geometrical center, x and y coordinates), and then for each specific question, the average area and centroid point (both x and y coordinates) were calculated over the readers. For the area measurement, precision was defined as the mean value of absolute differences between each reader's calculated area and the average area, and was calculated for each specific question. For the centroid measurements, precision was determined as the mean value of the Euclidean distances between each reader's centroid point and the average centroid, and was calculated for each question using the formulas in Eq. (3). The overall precision, as well as the reliability and the agreement between the readers were evaluated.

$$\text{Precision area} = \frac{\sum_{i=1}^3 \text{abs}(Area_i - \overline{Area})}{3}, \quad \text{where } \overline{Area} = \frac{\sum_{i=1}^3 Area_i}{3}$$

$$\text{Precision centroid} = \frac{\sum_{i=1}^3 \text{abs}(Distance_{ci})}{3},$$

$$\text{where } Distance_{ci} = \sqrt{(x_{ci} - \bar{x}_c)^2 + (y_{ci} - \bar{y}_c)^2 + (z_{ci} - \bar{z}_c)^2} \quad (3)$$

2.4. Placing multiple dots at the position of 3D landmarks

The readers were asked to place three dots on three landmarks: the tips of two transverse and spinous processes of a selected (T9) vertebra. For each question, the coordinates of the average dot were calculated over the readers. The precision in the 3D landmark positioning was determined by the mean value of the Euclidean distances between each reader's placed dot (x, y, z coordinates) and the average dot, and was calculated for each specific question using Eq. (4). The overall precision was evaluated.

$$\text{Precision} = \frac{\sum_{i=1}^3 \text{abs}(Distance_i)}{3}, \quad \text{where } Distance_i = \sqrt{(x_i - \bar{x})^2 + (y_i - \bar{y})^2 + (z_i - \bar{z})^2}, \quad (4)$$

where $(\bar{x}, \bar{y}, \bar{z})$ – the coordinates of the average dot: $\bar{x} = \frac{\sum_{i=1}^3 x_i}{3}$, $\bar{y} = \frac{\sum_{i=1}^3 y_i}{3}$, $\bar{z} = \frac{\sum_{i=1}^3 z_i}{3}$.

3. Results

It was feasible to obtain the MRI and sCT images in all volunteers. An

example of the experimental MRI images, acquired using the proposed short protocol, is presented in Fig. 2.

The mean Likert-based scores among the readers over different parameters are reported in Table 2. Most of the answers (>91 %) had a score ≥ 4 , which indicated moderate to high confidence of the readers in identifying all relevant parameters in the images.

The average precision calculated for the reader's measurements is presented in Table 3. The values indicate that the readers' answers were

Table 2

Scores of 3 readers over different parameters: Mean score, percentage with assessments 4 & 5. The following Likert-scale was used: 1. Poor confidence, impossible to detect/identify/classify; 2. Low confidence, doubtful to detect/identify/classify; 3. Neutral confidence, possible to detect/identify/classify; 4. Moderate confidence, definite detection/identification/classification possible; 5. High confidence, exact detection/identification/classification possible.

Parameter	Mean score \pm SD	Score ≥ 4 (%)	Score = 5 (%)
Identification of the Apical vertebral level	5.0 \pm 0.0	100	100
Classification of the IVD degeneration according to the Pfirrmann grade	4.5 \pm 0.5	100	54
Detection of underlying congenital vertebral anomalies	4.8 \pm 0.4	98	85
Determination of the 3D orientation of the pedicle for thoracic spine	4.8 \pm 0.6	91	87
Visualization of the surface of the posterior elements (base of spinous process, posterior surface of Lamina, posterior surface of transverse process) for surgical navigation for thoracic spine	4.9 \pm 0.3	100	91
Determination of the 3D orientation of the pedicle for lumbar spine	5.0 \pm 0.3	98	98
Visualization of the surface of the posterior elements (base of spinous process, posterior surface of Lamina, posterior surface of transverse process) for surgical navigation for lumbar spine	5.0 \pm 0.1	100	98
Detection of Presence/absence of the underlying neural axis abnormalities: Chiari malformation	5.0 \pm 0.0	100	100
Detection of Presence/absence of the underlying neural axis abnormalities: syringomyelia	5.0 \pm 0.0	100	100
Detection of Presence/absence of the underlying neural axis abnormalities: tethered cord	4.9 \pm 0.4	100	100

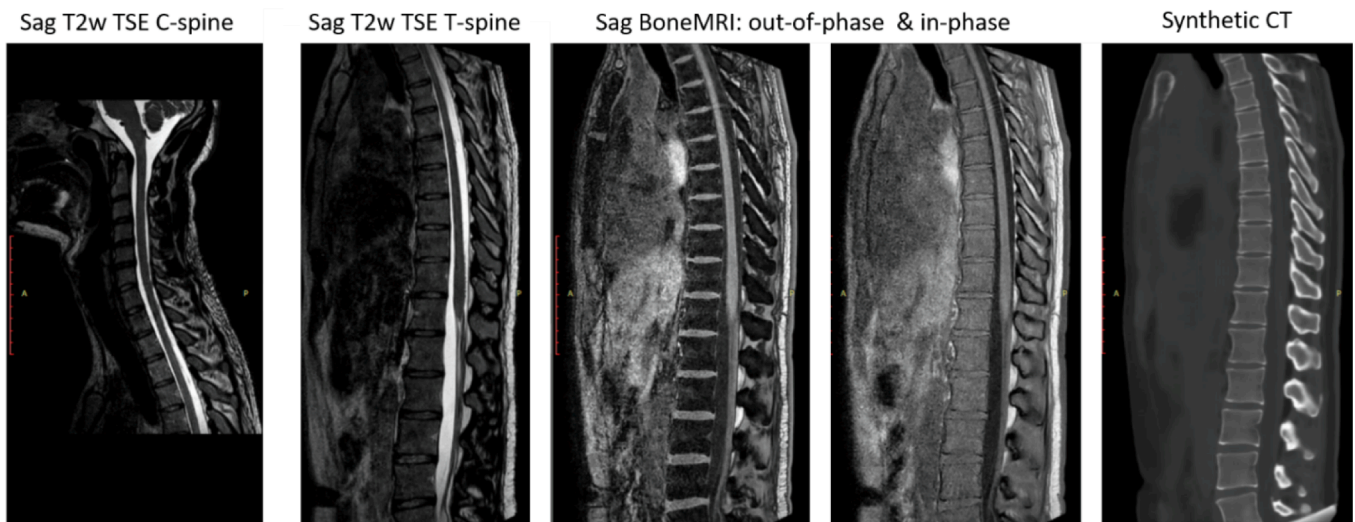


Fig. 2. MR images acquired in one volunteer: 3D Sag T2w TSE of C-spine and T-spine, BoneMRI source out-of-phase and in-phase images and the reconstructed synthetic CT images.

Table 3
Average precision, calculated for different readers' measurements.

Reader's measurement	Average precision
3D dot position	1.04 ± 0.6 mm
Angle	0.6 ± 0.3 degrees
Vertebral height	0.4 ± 0.2 mm
IVD height	0.4 ± 0.2 mm
NP area	8.5 ± 7.1 mm ²
IVD area	17.9 ± 15.6 mm ²
NP centroid	1.3 ± 1.1 mm
IVD centroid	1.1 ± 0.8 mm

close to each other on the angle measurement, 3D dot positioning, the vertebral and IVD height measurements, and on the measurements of the NP and IVD centroids. The precision values calculated for the NP and IVD area show greater variability between the readers' measurement. The ICC values and corresponding 95 % confidence intervals calculated for all relevant clinical parameters, are reported in Table 4. The values indicate excellent reliability of the angle measurement, vertebral and IVD height measurement, and good to excellent reliability for the calculated centroid of the NP and the IVD. However, for the both NP and the IVD area measurement the values indicate moderate reliability [33].

The results of the assessment of the agreement between the readers are shown in Fig. 3. Combined Jones plots are used to visualize the results. In the angle measurement, the mean difference between the readers is -0.34 degrees, which indicates a slight bias between the readers. However, the range of the limits of agreement is [-2.67; +2.18] degrees, which is relatively narrow, suggesting that the readers' measurements are generally in good agreement. The majority of data points fall within the limits of agreement. This suggests that while there may be individual discrepancies, the overall agreement is acceptable. In the height measurement, the mean difference between the readers is almost zero (0.02 mm), which shows no bias. The average measured vertebral and IVD heights were 21 mm and 4 mm correspondingly. The limits of agreement are [-1.76; +1.80] mm, which indicates a reasonable level of agreement. The majority of data points are scattered within the limits of agreement. The average measured NP area was 48 mm², the average measured IVD area was 164 mm². In the NP area measurement, the mean difference between the readers is 7.58 mm², indicating a slight positive bias, and the limits of agreement are quite wide, [-26.98; +42.14] mm², which indicates a considerable variability in the measurement agreement. In the IVD area measurement, the mean difference between the readers is 17.50 mm², indicating again a positive bias. The limits of agreement are very wide, [-55.62; +90.61] mm². This suggests considerable disagreement among the readers when placing an ROI on the IVD area. In the NP x-centroid measurement, the mean difference between the readers is 0.40 mm, with limits of agreement [-5.13; +5.94] mm. It suggests good agreement for the x-center measurement. The distribution of data points does not show any bias. In the NP y-centroid measurement, the mean difference between the readers is -0.04 mm and limits of agreement are [-1.92; +1.84] mm, indicating an excellent agreement. In the IVD x- and y-centroid measurement, both show relatively narrow limits of agreement and mean differences close

to zero. This suggests good agreement among the readers for these measurements.

4. Discussion

In this study in healthy volunteers, we have demonstrated a good feasibility and reproducibility of the proposed short MRI protocol for assessment of 3D morphology in scoliosis development, screening for neural axis abnormalities, pre-operative planning as well as surgical navigation. The protocol covers the complete cervical spine by a T2-weighted sequence with a 28 cm FOV, and thoracic and lumbar spine by both a T2-weighted and a sCT sequences with a 42 cm FOV within 14 min.

Our results showed that the readers had moderate to high confidence in identifying all relevant landmarks in the images. The agreement between the readers varied depending on the type of measurement. The measurements of the angle, IVD and vertebral height, NP and IVD centroids show an excellent agreement, while the measurements of NP and IVD areas show greater variability. The most probable source of this discrepancy is that placing a hand drawn ROI on the image is not an easy task and that the observers experienced difficulty in the differentiation of longitudinal ligaments to the NP at the level of the disc. This might be improved with additional instructions, which were not provided. An example of the contours drawn by three readers on two volunteer MRI images is shown in Fig. S1 in Supplementary material, which shows clear differences between the ROIs drawn by different readers. However, we still consider that observed variabilities in the area measurements fall within acceptable clinical and research standards. The reported values for the average precision in the measurements depend on the type of measurement as well. Taking into account that the reconstruction voxel size of the sCT images was $0.625 \times 0.625 \times 1$ mm³, and therefore the maximum distance in 3D between two adjacent voxels is 1.33 mm, the average precision in 3D dot positioning of 1 mm can be considered as high. The same conclusion comes from the reported precision values for NP and IVD centroid measurements, which fall under 0.9 mm. The average precision of 0.6° in angle measurement can be considered as high, considering other studies report Cobb angle measurement errors up to 3°. Moreover, the accepted standard error that represents a true change in spinal curvature is considered to be 5°, and the average angulation error of spinal navigation systems is approximately 2–6° [34,35]. The average precision of 0.4 mm in the measured vertebral height is 2 % of the mean measured vertebral height and therefore can be considered as high precision. For the measured IVD height, the precision of 0.4 mm is 10 % of the mean measured IVD height and can be considered as acceptable. For all types of measurements, except for the area measurements, the provided quantitative results showed good to excellent reliability. The area measurement values showed moderate reliability. To our knowledge, the evaluated precision, agreement and reliability between readers' measurements are sufficient for clinical implementation of this scan protocol.

The goal of this study was to develop a single-imaging-modality protocol, which would replace several different types of imaging which currently AIS patient often undergo. The proposed MRI protocol provides a 'one-size-fits-all' solution: in one short radiation-free examination both MRI and sCT images are obtained, revealing all relevant information on the bones, spinal soft-tissues and neurological structures, and bearing significant advantages both for the patient, their families, the hospital system and scoliosis researchers. To our knowledge, this is the first AIS protocol that combines both MRI and CT-like images in one modality. During scoliosis treatment and management, many clinical experts with different backgrounds, such as orthopedic or neurosurgeons, radiologists, rehabilitation specialists, orthotists and scoliosis exercise therapists are involved. Furthermore, most scoliosis surgeons present the obtained images to the patients. Therefore, ideally, the protocol should provide easily interpretable images without the need for a lot of training, experience, or expertise. The analysis showed that the

Table 4
Results of reliability assessment: the Intraclass Correlation Coefficient and the confidence interval, calculated for different clinical parameters.

Clinical Parameter	ICC	95 % Confidence Interval
Angle	0.985	[0.981, 0.988]
Vertebral and IVD Height	0.995	[0.993, 0.996]
NP area	0.549	[0.396, 0.688]
NP x-centroid	0.876	[0.814, 0.921]
NP y-centroid	0.924	[0.884, 0.953]
IVD area	0.615	[0.472, 0.738]
IVD x-centroid	0.906	[0.857, 0.941]
IVD y-centroid	0.877	[0.816, 0.922]

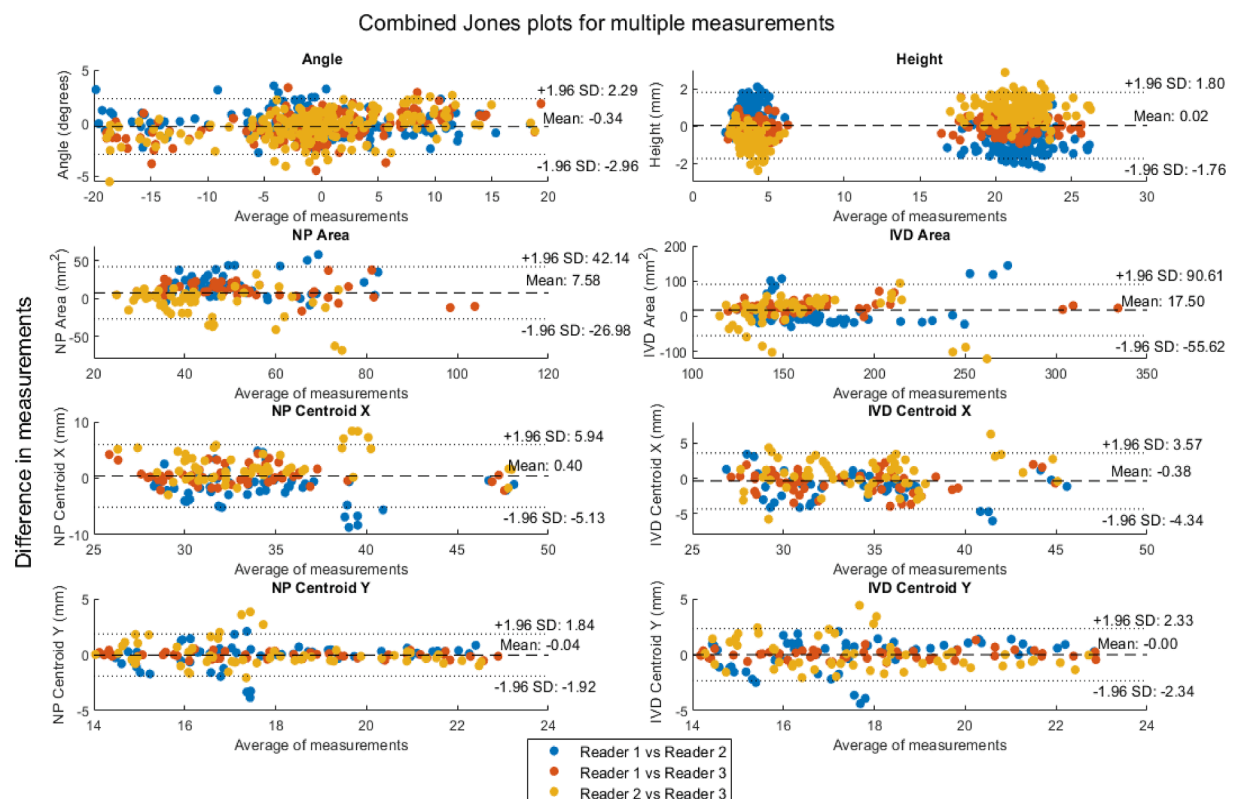


Fig. 3. Combined Jones plots for all types of measurements to assess the agreement between the readers on the measurement of clinically relevant parameters: angle, height, NP and IVD area, NP and IVD centroid. Each pair of readers can be distinguished in the plot with a different colour.

three readers with different clinical backgrounds and various levels of experience show high levels of precision, reliability, and agreement on landmark detection and image quality assessment. Thus, the protocol seems to fulfill this need.

4.1. Limitations

One of the limitations of this study is that the scanned volunteers are older than the general AIS population. AIS is normally seen mostly in adolescents during their growth spurt, and it is possible that MRI images and generated synthetic CT images might look differently in this younger population. In our future studies, scanning young individuals using the proposed protocol could give more insight into the aspects of AIS in this younger population.

Another limitation is that the 3D Sag T2-weighted sequence is not accurate enough for the detection of small intraspinal and filum lipomas that might be clinically relevant. A Sag T1-weighted sequence is still needed for that, and in principle, can always be added to the protocol. However, if the scanning time is limited, synthetic T1-weighted contrast imaging might be an alternative [36].

Furthermore, in this study only healthy volunteers participated, and no patients with neural axis abnormalities were included. In our future studies, we will investigate whether all relevant neural axis abnormalities can be detected using the proposed protocol in clinical practice.

Finally, while two volunteers showed a mild scoliosis, most individuals in this population did not have a scoliosis. With severe scoliosis, the width of the field of view might need to be increased to capture all desired landmarks, especially in double curves. In this case, an increased field of view might lead to a longer scanning time.

4.2. Improvements

One of the potential improvements of the proposed protocol is its

further acceleration. Based on our investigation of the lumbar spine [37], a potential 30 % decrease in acquisition time can be achieved by applying Compressed Sensing – SENSE to the BoneMRI sequence. In addition, novel acceleration techniques [38–40] might also be applied to the 3D T2-weighted TSE sequences, and can be further investigated.

Future studies should explore the applications of the proposed protocol in a broader clinical context, including its effectiveness in patients with moderate to severe scoliosis requiring treatment, in patients with braces and within spinal navigation software.

5. Conclusion

The proposed short MRI protocol fulfills its purposes for assessment of 3D morphology in scoliosis development, screening for neural axis abnormalities, pre-operative planning as well as surgical navigation.

Funding

This research was financially supported by the European Research Council (Grant no: 101020004).

CRediT authorship contribution statement

Yulia M. Shcherbakova: Data curation, Formal analysis, Investigation, Methodology, Resources, Software, Validation, Visualization, Writing – original draft, Writing – review & editing. **Peter P.G. Lafranca:** Data curation, Formal analysis, Methodology, Resources, Software, Visualization, Writing – review & editing. **Wouter Foppen:** Data curation, Formal analysis, Writing – review & editing. **Tijl A. van der Velden:** Data curation, Formal analysis, Resources, Software, Writing – review & editing. **Rutger A.J. Nievelstein:** Writing – review & editing. **Rene M. Castelein:** Conceptualization, Methodology, Writing – review & editing. **Keita Ito:** Conceptualization, Funding

acquisition, Methodology, Project administration, Supervision, Writing – review & editing. **Peter R. Seevinck:** Supervision, Writing – review & editing, Conceptualization, Methodology. **Tom P.C. Schlosser:** Conceptualization, Data curation, Formal analysis, Methodology, Supervision, Validation, Writing – review & editing.

Declaration of competing interest

The authors declare that they have no known competing financial interests or personal relationships that could have appeared to influence the work reported in this paper.

Appendix A. Supplementary material

Supplementary material to this article can be found online at <https://doi.org/10.1016/j.ejrad.2024.111542>.

References

- [1] S.L. Weinstein, L.A. Dolan, J.C. Cheng, et al., Adolescent idiopathic scoliosis, *Lancet* 371 (2008) 1527–1537, [https://doi.org/10.1016/S0140-6736\(08\)60658-3](https://doi.org/10.1016/S0140-6736(08)60658-3).
- [2] J.C. Cheng, R.M. Castelein, W.C. Chu, et al., Adolescent idiopathic scoliosis, *Nat. Rev. Dis. Prim.* 1 (2015), <https://doi.org/10.1038/nrdp.2015.30>.
- [3] S.L. Weinstein, The natural history of adolescent idiopathic scoliosis, *J. Pediatr. Orthop.* 39 (2019) S44–S46, <https://doi.org/10.1097/BPO.0000000000001350>.
- [4] M. Inoue, S. Minami, Y. Nakata, et al., Preoperative MRI analysis of patients with idiopathic scoliosis, *Spine (Phila Pa 1976)* 30 (2005) 108–114, <https://doi.org/10.1097/01.brs.0000149075.96242.0e>.
- [5] İ.T. Benli, O. Üzümcügil, E. Aydın, et al., Magnetic resonance imaging abnormalities of neural axis in lenke type 1 idiopathic scoliosis, *Spine (Phila Pa 1976)* 31 (2006) 1828–1833, <https://doi.org/10.1097/01.brs.0000227256.15525.9b>.
- [6] M. Diab, Z. Landman, J. Lubicky, et al., Use and outcome of MRI in the surgical treatment of adolescent idiopathic scoliosis, *Spine (Phila Pa 1976)* 36 (2011) 667–671, <https://doi.org/10.1097/BRS.0b013e3181da218c>.
- [7] R.R. Murgai, B. Tamrazi, K.D. Illingworth, et al., Limited sequence MRIs for early onset scoliosis patients detected 100% of neural axis abnormalities while reducing MRI time by 68%, *Spine (Phila Pa 1976)* 44 (2019) 866–871, <https://doi.org/10.1097/BRS.0000000000002966>.
- [8] M.M. Rehani, Radiation doses in computed tomography, *BMJ* 320 (2000) 593–594, <https://doi.org/10.1136/bmj.320.7235.593>.
- [9] D.J. Brenner, E.J. Hall, Computed Tomography — An Increasing Source of Radiation Exposure, *N. Engl. J. Med.* 357 (2007) 2277–2284, <https://doi.org/10.1056/NEJMr072149>.
- [10] A. Duke, R. Marchese, D.E. Komatsu, J. Barsi, Radiation in adolescent idiopathic scoliosis management: estimated cumulative pre-operative, intra-operative, and post-operative exposure, *Orthop. Res. Rev.* 14 (2022) 487–493, <https://doi.org/10.2147/ORR.S387369>.
- [11] B.M. Striano, A.M. Crawford, B.P. Verhofste, et al., Intraoperative navigation increases the projected lifetime cancer risk in patients undergoing surgery for adolescent idiopathic scoliosis, *Spine J.* (2024), <https://doi.org/10.1016/j.spinee.2024.01.007>.
- [12] D.J. Brenner, C.D. Elliston, E.J. Hall, W.E. Berdon, Estimated risks of radiation-induced fatal cancer from pediatric CT, *Am. J. Roentgenol.* 176 (2001) 289–296, <https://doi.org/10.2214/ajr.176.2.1760289>.
- [13] M.S. Pearce, J.A. Salotti, M.P. Little, et al., Radiation exposure from CT scans in childhood and subsequent risk of leukaemia and brain tumours: a retrospective cohort study, *Lancet* 380 (2012) 499–505, [https://doi.org/10.1016/S0140-6736\(12\)60815-0](https://doi.org/10.1016/S0140-6736(12)60815-0).
- [14] D.L. Miglioretti, E. Johnson, A. Williams, et al., The use of computed tomography in pediatrics and the associated radiation exposure and estimated cancer risk, *JAMA Pediatr.* 167 (2013) 700–707, <https://doi.org/10.1001/jamapediatrics.2013.311>.
- [15] N.M.Y. Journy, C. Lee, R.W. Harbron, et al., Projected cancer risks potentially related to past, current, and future practices in paediatric CT in the United Kingdom, 1990–2020, *Br. J. Cancer* 116 (2017) 109–116, <https://doi.org/10.1038/bjc.2016.351>.
- [16] M. Bosch, D.B. Gomez, I. Thierry-chef, et al., Risk of hematological malignancies from CT radiation exposure in children, adolescents and young adults, 2023. Doi: <https://doi.org/10.1038/s41591-023-02620-0>.
- [17] Toetsingskader Onderzoek met Minderjarige Proefpersonen (Assessment Framework for Research with Minor Participants) Author/Organization: Centrale Commissie Mensgebonden Onderzoek (CCMO) – Netherlands, 2017.
- [18] M.C. Florkow, F. Zijlstra, K. Willemsen, et al., Deep learning-based MR-to-CT synthesis: The influence of varying gradient echo-based MR images as input channels, *Magn. Reson. Med.* 83 (2020) 1429–1441, <https://doi.org/10.1002/mrm.28008>.
- [19] L. Morbée, M. Chen, T. Van Den Berghe, et al., MRI-based synthetic CT of the hip: can it be an alternative to conventional CT in the evaluation of osseous morphology? *Eur. Radiol.* 32 (2022) 3112–3120, <https://doi.org/10.1007/s00330-021-08442-3>.
- [20] B. (Britt) Y.M. van der Kolk, D.J. (Jorik) Slotman, I.M. Nijholt, et al., Bone visualization of the cervical spine with deep learning-based synthetic CT compared to conventional CT: A single-center noninferiority study on image quality, *Eur. J. Radiol.* 154 (2022) 110414, <https://doi.org/10.1016/j.ejrad.2022.110414>.
- [21] L.B.O. Jans, M. Chen, D. Elewaut, et al., MRI-based synthetic CT in the detection of structural lesions in patients with suspected sacroiliitis: comparison with MRI, *Radiology* 298 (2021) 343–349, <https://doi.org/10.1148/radiol.2020201537>.
- [22] L. Morbée, E. Vereecke, F. Laloo, et al., Common incidental findings on sacroiliac joint MRI: added value of MRI-based synthetic CT, *Eur. J. Radiol.* 158 (2023) 110651, <https://doi.org/10.1016/j.ejrad.2022.110651>.
- [23] E. Schiettecatte, E. Vereecke, J.L. Jaremko, et al., MRI-based synthetic CT for assessment of the bony elements of the sacroiliac joints in children, *Insights Imaging* 15 (2024) 53, <https://doi.org/10.1186/s13244-023-01603-6>.
- [24] L. Morbée, M. Chen, N. Herregods, et al., MRI-based synthetic CT of the lumbar spine: Geometric measurements for surgery planning in comparison with CT, *Eur. J. Radiol.* 144 (2021), <https://doi.org/10.1016/j.ejrad.2021.109999>.
- [25] A.D. Davidar, B.F. Judy, A.M. Hersh, et al., Robot-assisted screw fixation in a cadaver utilizing magnetic resonance imaging–based synthetic computed tomography: toward radiation-free spine surgery. Illustrative case, *J. Neurosurg Case Lessons* 6 (2023), <https://doi.org/10.3171/CASE23120>.
- [26] V.E. Staartjes, P.R. Seevinck, W.P. Vandertop, et al., Magnetic resonance imaging–based synthetic computed tomography of the lumbar spine for surgical planning: a clinical proof-of-concept, *Neurosurg. Focus* 50 (2021) 1–7, <https://doi.org/10.3171/2020.10.FOCUS20801>.
- [27] J. Upadhyay, J. Iwasaka-Neder, E. Golden, S. Bixby, Synthetic CT assessment of lesions in children with rare musculoskeletal diseases, *Pediatrics* 152 (2023), <https://doi.org/10.1542/peds.2022-061027>.
- [28] Iwasaka-Neder et al., Hip MRI-Based Synthetic CT Versus Conventional CT: A Morphometric and Clinical Comparison in Young Patients, in: *RSNA*, 2023.
- [29] Schiettecatte et al., BoneMRI of sacroiliac joints in children, in: *ESSR*, 2023.
- [30] K.L. Vincken, C.J.M.C. Ravesloot, Vquest, Computer software, 2010.
- [31] D. Liljequist, B. Elfving, K. Skavberg Roaldsen, Intraclass correlation – A discussion and demonstration of basic features, *PLoS One* 14 (2019) e0219854.
- [32] M. Jones, A. Dobson, S. O'Brian, A graphical method for assessing agreement with the mean between multiple observers using continuous measures, *Int. J. Epidemiol.* 40 (2011) 1308–1313, <https://doi.org/10.1093/ije/dyr109>.
- [33] T.K. Koo, M.Y. Li, A guideline of selecting and reporting intraclass correlation coefficients for reliability research, *J. Chiropr. Med.* 15 (2016) 155–163, <https://doi.org/10.1016/j.jcmm.2016.02.012>.
- [34] T. Vrtovec, F. Pernuš, B. Likar, A review of methods for quantitative evaluation of spinal curvature, *Eur. Spine J.* 18 (2009) 593–607, <https://doi.org/10.1007/s00586-009-0913-0>.
- [35] S. Youssef, J.M. McDonnell, K.V. Wilson, et al., Accuracy of augmented reality-assisted pedicle screw placement: a systematic review, *Eur. Spine J.* (2024), <https://doi.org/10.1007/s00586-023-08094-5>.
- [36] T. Zhou, H. Fu, G. Chen, et al., Hi-Net: Hybrid-fusion network for multi-modal MR image synthesis, *IEEE Trans. Med. Imaging* 39 (2020) 2772–2781, <https://doi.org/10.1109/TMI.2020.2975344>.
- [37] Y. Shcherbakova, T. van der Velden, P.R. Seevinck, Does CS-SENSE acceleration influence the performance of an AI based synthetic CT algorithm? A volunteer study in the lumbar spine. Proceedings of the Annual Meeting of ISMRM in Toronto, Canada, 2023. Program Number 3107.
- [38] N. Kashiwagi, M. Sakai, A. Tsukabe, et al., Ultrafast cervical spine MRI protocol using deep learning-based reconstruction: Diagnostic equivalence to a conventional protocol, *Eur. J. Radiol.* 156 (2022) 110531, <https://doi.org/10.1016/j.ejrad.2022.110531>.
- [39] K.M. Awan, A.L.M. Goncalves Filho, A. Tabari, et al., Diagnostic evaluation of deep learning accelerated lumbar spine MRI, *Neuroradiol. J.* (2024), <https://doi.org/10.1177/19714009231224428>.
- [40] M. Zerunian, F. Pucciarelli, D. Caruso, et al., Fast high-quality MRI protocol of the lumbar spine with deep learning-based algorithm: an image quality and scanning time comparison with standard protocol, *Skeletal Radiol.* 53 (2024) 151–159, <https://doi.org/10.1007/s00256-023-04390-9>.